The *ab initio* calculation for Li_2F and Na_2F systems

Yue Wang*, Bi Lv Fang, Yu Liu,
De Zhi Dong, Gan Gao and Cheng Wen Zhang

Department of Electrical Engineering, Tongling University, 1335 Cuihu 4th Road, 244000, Tongling, China

Received: 21.03.2021 & Accepted: 06.09.2022

Doi: 10.12693/APhysPolA.142.473 *e-mail: wangyue8001@qq.com

The globally accurate potential energy surface for the ground state of Li_2F and Na_2F systems was presented using the coupled-cluster singles and doubles excitation approach with perturbation treatment of triple excitations. Mixed basis sets were applied, aug-cc-pCVQZ for the lithium and sodium atoms and aug-cc-pCVDZ for the fluoride atom, with midbond functions ($3s3p2d$). In total, about 2080 points were generated for three-dimensional surfaces. Both the Li_2F and Na_2F molecules were confirmed to be bent at equilibrium. For Li–F–Li with an angle of 90°, the depth of the potential well is 3.87 eV at $R = 2a_0$, and the height of the barrier required to linearity with 0° angle equals 285.76 eV at $R = 5.6a_0$. For Na–F–Na with an angle of 90°, the depth of the potential well is 5.289 eV at $R = 3a_0$, and the height of the barrier required to linearity with 0° angle equals 721 eV at $R = 2.6a_0$. Our *ab initio* calculations of potential surface and potential energy surface were compared with the experimental results.

topics: Li_2F and Na_2F systems, potential energy surface, *ab initio* calculation, CCSD(T)

1. Introduction

Since the 1990s, the technology of laser cooling and trapping neutral atoms has been greatly developed, which provides conditions for the realization of the miracle of Bose–Einstein condensation (BEC) and sets off the upsurge in the research of ultracold atomic and molecular physics. Encouraged by the BEC experiments of alkali atomic gases, studies of cold collisions between alkali and metal have developed rapidly [1–5]. Because Li and Na atoms are light alkali metal atoms, it is of great significance to study the cold collision characteristics of Li_2 and Na_2 associated with alkali metal diatoms for the research and application of cold molecular physics [6–8]. Using *ab initio* quantum mechanics, scientists have obtained more accurate spectral data of alkali metal diatomic molecules, which provides a basis for further study of the potential energy functions of triatomic and polyatomic molecules [9–11].

On the other hand, fluoride is a mostly symmetrical structure, with minimal intermolecular coupling, a small molecular weight of fluoride itself, and low intermolecular attraction. Such a small intermolecular force makes the interaction between fluorine atoms and other atoms relatively weak, which creates difficulties for experimental detection and theoretical research.

The Li_2F and Na_2F systems belong to super valence compounds containing odd electrons, and they have good nonlinear optical properties, so the scientific study of the supermolecular structure of alkali metal fluoride has always shown a strong interest in Li_2F and Na_2F system [12–15].

In the past years, the reaction kinetics of Li_2F and Na_2F systems have been researched using many different methods. For example, there are quite a few experimental data about the ground state and excited state energy surface of Li_2F and Na_2F systems [16–19]. In this work, we first analyzed the dissociation limit of the ground state of Li_2F and Na_2F molecules and then calculated the interaction potential. Finally, we produced the full-dimensional (3D) global potential energy surface (PES) for Li_2F and Na_2F systems.

2. Method of Calculation

2.1. The limit of ground state of X_2F molecular dissociation

In order to obtain the X_2F molecular potential energy function of the ground state, first of all, we need to make sure that the system has a reasonable dissociation limit. Both the X and F atoms belong to SO(3), and their ground state electron states are ^2S_g and ^2P_u, respectively. The XF molecules

belong to the $C_{\infty v}$ group, and their ground state electron state is $^1\Sigma^+$. The X_2 molecule belongs to the $D_{\infty h}$ group, and its ground state electron state is $^1\Sigma_g^+$. The Li_2F and Na_2F molecules belong to the C_{2V} group. By the microscopic reversibility principle of the process and the optimal energy principle, we have the X molecular dissociation limit A, as follows from

$$X_2F(X^2A_1) \rightarrow \begin{cases} F(^2P_u) + X_2(X^1\Sigma_g^+) \\ XF(X^1\Sigma^+) + X(^2S_g) \\ X(^2S_g) + X(^2S_g) + F(^2P_u) \end{cases} \quad (1)$$

2.2. Sampling of *ab initio* points and analytical the PES

We calculated the energy of correlated valence electrons and all correlated electrons. The calculations have been performed using the Gaussian 09W package [20]. We used the coupled-cluster singles and doubles excitation approach with the perturbative treatment of triple excitations [CCSD(T)] method.

The single point energy calculation and geometric optimization (including optimization to transition states) are the most common types of tasks. The sensitivity of geometric optimization to the basis group is much lower than that of the calculation of single point energy, and the time of geometric optimization is ten times, dozens of times, or even hundreds of times longer than that of the single point calculation, so the geometric optimization absolutely does not need large basis group. In this study, we adopted the basis set aug-cc-pCVQZ for the lithium and sodium atoms and aug-cc-pCVDZ for the fluoride atom. It is well known that mid-bond functions are necessary to improve the basis set convergence, so we placed the mid-bond functions (3*s*3*p*2*d*) (for 3*s* 0.9, 3*p* 0.3, and 2*d* 0.2) in the center of the origin of coordinates and fluorine atom, which trajectory as a hemispheroid is shown in Fig. 1. We performed our quantum analysis in the framework of the Jacobi coordinates system (r, R, θ, ϕ).

In Fig. 1, r is the distance of X–X (X = Li and Na), R is the length of the vector connecting the X–X center of mass and the F atom, and θ is the angle between this vector and the X–X bond, ϕ is the angle between r and z axis. For a given value of R, the angle θ and ϕ change from 0° to 180° in steps of 10°.

We have to add diffuse augmentation functions on X (X=Li and Na) when calculating to ensure that the basis permits polarization by X. We use the experimentally determined equilibrium value of $r_{Li} = 2.604a_0$ and $r_{Na} = 3.228a_0$ [21]. In the barrier and the well range ($0.2a_0 \le R \le 5.8a_0$), we fixed in steps of $\Delta R = 0.2a_0$. In the long range ($6a_0 \le R \le 12a_0$) we used equally spaced grids with $\Delta R = 1a_0$. The interaction energy is calculated for 2080 geometries.

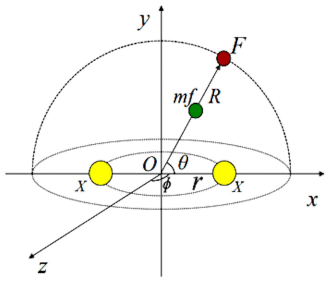

Fig. 1. Geometric configuration of the system.

We used the standard definition of the direct product of irreducible tensors. The system of multi-body expansion for the potential energy function is the following expression

$$V(r, R, \theta) = V_w(r, R, \theta) + V_l(r, R, \theta) + V_b(r, R, \theta). \quad (2)$$

We define r by $r = r_i - r_e$. The function contains location of the potential well range V_w, the long range V_l, and the barrier range V_b. The well range and the barrier range include a damped-dispersion expansion.

The well part consists of the exponential functional form, which is as follows

$$V_w(r, R, \theta) = \sum_{n=6}^{9} \sum_{\substack{l=0,2... \\ l=1,3...}} \frac{f_6\big(D(\theta)R\big)C^l}{R^n} P_l^0\big(\cos(\theta)\big). \quad (3)$$

The long distance part is

$$V_l(r, R, \theta) = G(r, R, \theta)\, \mathrm{e}^{\big(B(r,\theta) - D(r,\theta)R\big)}. \quad (4)$$

We described the barrier range as

$$V_b(r, R, \theta) = \frac{f_6\big(B(r,\theta)R\big)}{R^6}\Big[C^0 + C^2\, P_1(\cos(\theta))\Big] + \frac{f_8\big(B(r,\theta)R\big)}{R^8} \times \Big[C^0 + C^2 P_1(\cos(\theta)) + C^4 P_2(\cos(\theta))\Big], \quad (5)$$

where the term $f_n(x)$ defined by

$$f_n(x) = 1 - e^{-x} \sum_{k=0}^{n} \frac{x^k}{k!}. \quad (6)$$

Note that $B(r, \theta)$, $D(r, \theta)$ and $G(r, R, \theta)$ all denote expansions in Legendre polynomials $P_l(\cos\theta)$ and they are defined as follows

$$B(r, \theta) = \sum_{l=0}^{L_1} b^l(r)\, P_l\big(\cos(\theta)\big), \quad (7)$$

$$D(r, \theta) = \sum_{l=0}^{L_1} d^l(r)\, P_l\big(\cos(\theta)\big), \quad (8)$$

$$G(r, R, \theta) = \sum_{l=0}^{L_2} \Big[g_0^l(r) + g_1^l(r)R + g_2^l(r)R^2 + g_3^l(r)R^3\Big]\, P_l\big(\cos(\theta)\big). \quad (9)$$

TABLE I

Molecular parameters for the analytic PES.

l	b_l	d_l	g_0^l	g_1^l	g_2^l	C^l
Parameters for Li_2F system						
0	2.2522×10^{-5}	-4.449×10^{-4}	9.285267×10^{-7}	-5.8051×10^{-6}	3.4281×10^{-5}	7.7472×10^{-8}
2	-3.0255×10^{-6}	-8.42097×10^{-6}	-4.20639×10^{-7}	6.5759×10^{-6}	-1.4252×10^{-7}	5.92125×10^{-8}
4	4.15075×10^{-7}	-3.6756×10^{-6}	1.03688×10^{-7}	-6.84453×10^{-7}	3.35458×10^{-6}	-8.0021×10^{-8}
6	4.3641×10^{-2}	-5.42471×10^{-2}	5.25331×10^{-3}	-1.20245×10^{-4}	-5.3535×10^{-2}	-3.6555×10^{-8}
8	6.1569×10^{-5}	-8.54675×10^{-4}	2.2534×10^{-3}	-8.98207×10^{-5}	2.455×10^{-4}	-1.15453×10^{-8}
Parameters for Na_2F system						
0	-5.142×10^{-7}	4.0311×10^{-6}	-1.15453×10^{-6}	-9.7212×10^{-6}	-4.5542×10^{-7}	4.93967×10^{-8}
2	-1.1411×10^{-5}	6.6443×10^{-5}	-4.047×10^{-4}	2.8005×10^{-6}	5.12415×10^{-5}	-1.09223×10^{-8}
4	9.56585×10^{-5}	-2.1053×10^{-7}	1.1054×10^{-6}	-7.5056×10^{-6}	-7.56855×10^{-5}	-6.46893×10^{-8}
6	3.7099×10^{-6}	2.50525×10^{-7}	1.6505×10^{-5}	-9.6142×10^{-5}	$3.956.9 \times 10^{-6}$	3.11746×10^{-8}
8	-4.0257×10^{-6}	2.457×10^{-5}	-1.0056×10^{-4}	2.7143×10^{-7}	-2.54747×10^{-6}	-4.72743×10^{-8}

Ab initio potential energies were fitted using the analytical symmetry-adapted representation (8)–(10) and represent a Legendre polynomial of order l. Considering the symmetry, only odd orders are allowed with $L_1 = 8$, $L_2 = 8$.

We present all the molecular parameters for the analytic PES in Table I. All the 2080 *ab initio* points on the two PESs are fitted respectively to a 30-parameter algebraic form. The maximum error for the Li_2F system is 0.0645% and the average absolute error is less than 0.00758%. And the maximum error for the Na_2F system is 0.0736% and the average absolute error is less than 0.00553%.

3. Results and discussion

Figure 2 presents the ground state potential energy curves of two systems at different angles. The potential energy curves of the two systems have the same general trend. As the angle increases, the peak values of the potential curves shift in the direction of R. The peak values decrease with the increase of the angle, and there is no obvious peak value at 90°. At every angle, the peak of the Li_2F system is always higher than the peak of the Na_2F system. There is no minimum value for the two systems in the 0–40° curve graph.

Valleys begin to appear from 50°, and the minimum values of the two systems all increase with the increase of angle. Both systems have a minimum value at 90°, which is the potential well. The potential well of the Na_2F system is a little deeper than that of the Li_2F system. It is because Na_2 diatoms bind fluorine atoms more strongly than Li_2 diatoms. The potential energy curves as a whole show strong anisotropy. For Li–F–Li with an angle of 90°, the depth of the potential well is 3.87 eV at $R = 2a_0$, which is close to that obtained from the experiment. The height of the barrier required to linearity for Li–F–Li with 0° angle equals 285.76 eV at $R = 5.6a_0$, which is also close to that obtained

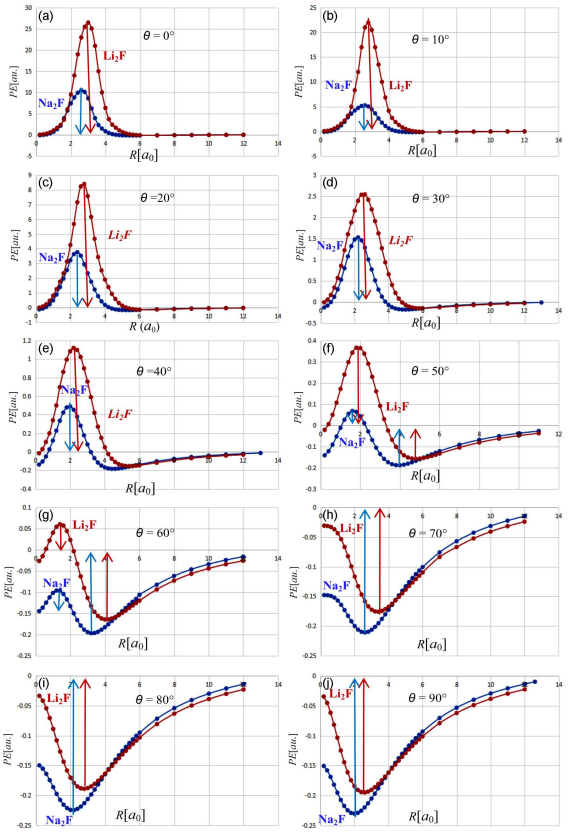

Fig. 2. Orientational features of the potential energy surface of Li_2F and Na_2F systems. Here, PE is potential energy, and panels (a–j) show the curve comparison of different angles.

from the experiment [22]. For Na–F–Na with an angle of 90°, the depth of the potential well is 5.289 eV at $R = 3a_0$, and that as well is in agreement with the experimental data [22]. The height of the barrier required to linearity for Na–F–Na with 0° angle equals 721 eV at $R = 2.6a_0$. Meanwhile, in the range, as the minimum values increase, the shifts towards the direction of the R decrease.

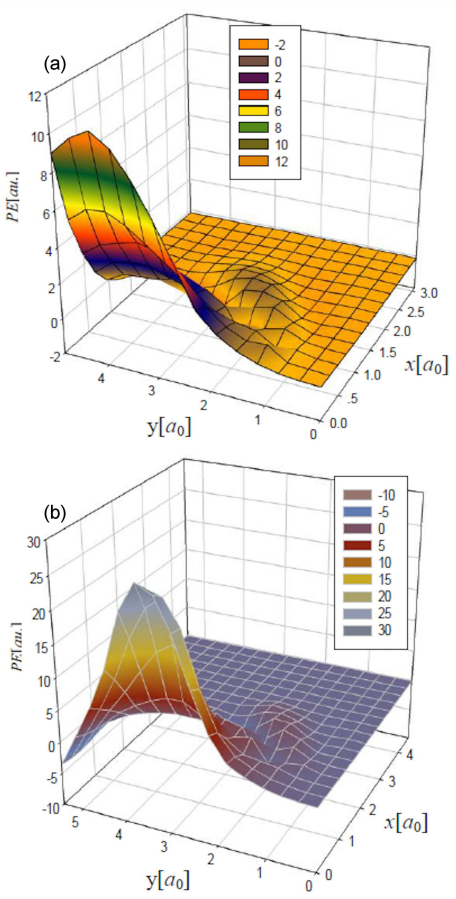

Fig. 3. 3D potential energy of 0–90° for (a) Li_2F and (b) Na_2F system.

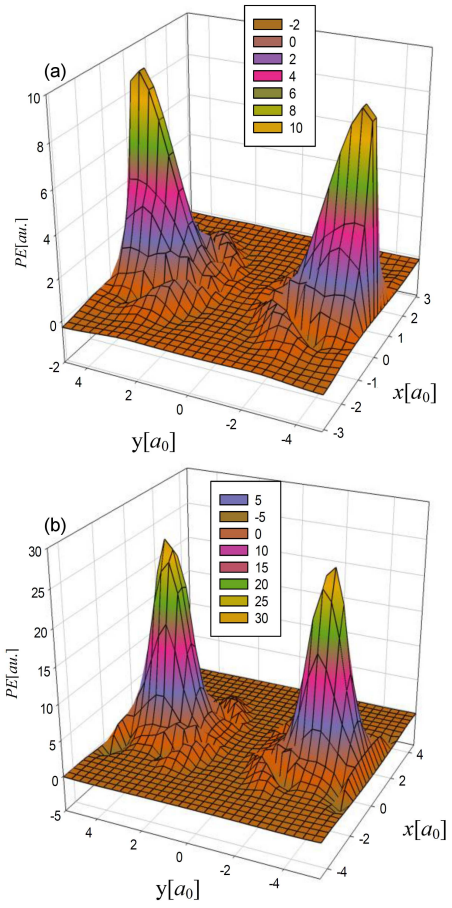

Fig. 4. 3D view of the interaction potential for (a) Li_2F and (b) Na_2F systems at $r = r_e$.

In Fig. 3, we show the three-dimensional potential energy surface of the two systems with angles of 0–90°. From the three-dimensional surface diagram, we find that those two systems have many common characteristics. The whole potential energy surface has strong anisotropy in the short-range region, which indicates isotropy in the long-range region. The Na_2F system has a bigger peak and a deeper valley, which may be related to molecular collisions and van der Waals forces.

In Table II, we present the results of Li_2F and Na_2F system calculations, along with the experimental data and previous computational results obtained for PESs [21–25]. The comparison of the characteristics of our fitted PES with the previous ones indicates that our theoretical results are in good agreement with the experimental data.

In Fig. 4, we show the new 3D view of the interaction potential for Li_2F and Na_2F systems of the ten angles θ = 0–180° and ϕ = 0–360° for the Li_2F and Na_2F systems. The comparison of the two systems shows that the overall trend of change is the same. We can clearly see that the saddle point is at $\theta = 0°$, and the barrier point is located at $\theta = 90°$.

TABLE II

Results of the calculations compared with the experimental data.

Li_2F system				
Parameters	Exper. data [23]	Ref. [22]	Ref. [24]	Our results
R_{Li-Li} [a_0]	2.722	2.644	2.67	2.696
D [eV]	3.8 ± 0.2	3.89	4.82	3.87
Relative error	–	2.37%	26.8%	1.58%
Na_2F system				
Parameters	Exper. data [25]	Ref. [21]	Our results	Relative error
R_{Na-Na} [a_0]	3.30	3.224	3.292	2.42%
D [eV]	5.3	5.72	5.289	0.21%

We can see that the PESs are smooth over the whole configuration space. There are two valleys on the surface, the left valley and the right valley, which correspond to the product of F+Li(Na)$_2$ and the reactant of Li(Na)–F–Li(Na), respectively. We can easily see the mainly isotropic interaction and the well-defined molecular core identified by the repulsive regions, which show vanishing angular dependence for this very weakly bound Van der Waals complex.

4. Conclusions

The *ab initio* calculation and equilibrium geometrical parameters of the X^2A_1 ground state of Li_2F and Na_2F systems are performed by CCSD(T) method using the aug-cc-pCVQZ/aug-cc-pCVDZ+332 basis set. The 3D PESs diagram clearly shows the equilibrium structure and characteristics of the radical molecules of Li_2F and Na_2F systems. We can get some common features, and by using these features, the correctness of the new function expression and parameters can not only be evaluated to develop new potential energy function models but also provide more information. Our calculations will provide the theoretical basis for cold collision between alkali metal diatomic molecules and halogen atoms.

Acknowledgments

The authors acknowledge the Key projects of science research in University of Anhui Province (grants KJ2020A0695, KJ2021A1059, KJ2020A0699), the College Students' innovative training program (grants tlxy2022103830001, tlxy2022103830004), Tongling University grassroots Party construction model branch project, the teaching demonstration class project in Anhui Province (grant 2020SJJXSFK2400), the Innovation Project of Excellent Talents Training in Anhui Province (grant 2020zyrc153), the First-class teaching material project in Anhui Province (grant 2020yljc127), the Key teaching research projects in Anhui Province (2021jyxm1547), Tongling University Student Research Project (grant 2021tlxydxs135).

References

[1] M. Gutowski, J. Simons, *J. Chem. Phys.* **100**, 1308 (1994).

[2] Z. Cao, H. Xian, W. Wu, Q. Zhang, *Chem. Phys.* **243**, 209(1999).

[3] Y. Wang, *Acta Phys. Pol. A* **119**, 354 (2011).

[4] D. Zanuttini, J. Douady, E. Jacquet, E. Giglio, B. Gervais, *J. Chem. Phys.* **134**, 044308 (2011).

[5] K. Hatua, A. Monda, P.K. Nandi, *Chem.Phys. Lett.* **686**, 16 (2017).

[6] Z.H. Wang, T. Chen, Y.C. Liu, J.X. Xing, A.J. Zhou, J.G. Li, W. Zoud, F. Zhoud, *Chem. Eng. J.* **430**, 3 (2022).

[7] Y.H. Ma, D. Li, H. Zhang, X. Feng C. Liang, *Phys. Lett. A* **384**, 126569 (2020).

[8] B.G.A. Britoa, G.-Q. Haib, L. Cândido, *Chem. Phys. Lett.* **708**, 54 (2018).

[9] A.K. Srivastava, *Chem. Phys. Lett* **759**, 138049 (2020).

[10] Z. Gao, X.L. Cheng, M.J. Zhao, *Comput. Theor. Chem.* **1214**, 113781 (2022).

[11] K. Yokoyama, N. Haketa, M. Hashimoto, K. Furukawa, H. Tanaka, H. Kudo, *Chem. Phys. Lett.* **320**, 645 (2000).

[12] K.Yokoyama, N. Haketa, H. Tanaka, K. Furukawa, H. Kudo, *Chem. Phys. Lett.* **330**, 339 (2000).

[13] R. Bano, M. Arshad, T. Mahmood, K. Ayub, A. Sharif, S. Tabassum, M.A. Gilani, *Mater. Sci. Semicond. Proc.* **143**, 106518 (2022).

[14] N. Hou, D. Wu, Y. Li, Z.-R. Li, *J. Am. Chem. Soc.* **136**, 2921 (2014).

[15] O. Neskovic, M. Veljkovic, S. Velickovic, *Rapid Commun. Mass Spectrom.* **17**, 212 (2003).

[16] Y. Wang, Y. Liu, B.L. Fang, G. Gao, C. Zhang, D. Dong, *Adv. Math. Phys.* **2022**, 1 (2022).

[17] A.K. Srivastava, N. Misra, *Mol. Phys.* **112**, 2621 (2014).

[18] A.K. Srivastava, N. Misra, *J. Mol. Model.* **22**, 122 (2016).

[19] H. Yang, Y. Li, D. Wu, Z.-R. Li, *Int. J. Quantum Chem.* **112**, 770 (2012).

[20] M.J. Frisch, G.W. Trucks, H.B. Schlegel et al., Gaussian 09 (now Gaussian 16), Gaussian Inc., Wallingford (CT) 2016.

[21] A.K. Srivastava, N. Misra, *Mol. Simulat.* **42**, 981 (2016).

[22] A.K. Srivastava, N. Misra, *J. Mol. Model.* **21**, 305 (2015).

[23] S.R. Veličković, V.J. Koteski, J.N. BeloševićČavor, *Chem. Phys. Lett.* **448**, 151 (2007).

[24] B. Somnath, H.R. Denis, G.H. Jeung, *J. Chem. Phys.* **145**, 034306 (2016).

[25] M.C. Heitz, G. Durand, F. Spiegelman, *J. Chem. Phys.* **118**, 1282 (2003).